Extreme ultraviolet interference lithography with incoherent light

Patrick P. Naulleau,[1] Christopher N. Anderson,[2] and Stephen F. Horne [3]

[1] Center for X-Ray Optics, Lawrence Berkeley National Laboratory, Berkeley, CA 94720
[2] Applied Science & Technology Department, University of California, Berkeley, CA 94720
[3] Energetiq Technology Inc., Woburn, MA 01801

ABSTRACT

In order to address the crucial problem of high-resolution low line-edge roughness resist for extreme ultraviolet (EUV) lithography, researchers require significant levels of access to high-resolution EUV exposure tools. The prohibitively high cost of such tools, even microfield tools, has greatly limited this availability and arguably hindered progress in the area of EUV resists. To address this problem, we propose the development of a new interference lithography tool capable of working with standalone incoherent EUV sources.

Although EUV interference lithography tools are currently in operation, presently used designs require illumination with a high degree of spatial and/or temporal coherence. This, in practice, limits current systems to being implemented at synchrotron facilities greatly restricting the accessibility of such systems. Here we describe an EUV interference lithography system design capable of overcoming the coherence limitations, allowing standalone high-power broad sources to be used without the need for excessive spatial or temporal filtering. Such a system provides promising pathway for the commercialization of EUV interference lithography tools.

Keywords: extreme ultraviolet, lithography, interferometry, coherence

1. INTRODUCTION

One of the largest challenges facing the commercialization of EUV lithography [1] is the development of high resolution EUV resists. Progress in this area has been hampered in large part due to the scarcity in availability of high-resolution EUV tools. Presently only three high numerical aperture (0.25 or greater) projection EUV tools are available for general use [2-4]. Additionally, only two synchrotron-based interference lithography tools are operational [5, 6]. The key to alleviating the shortfall in EUV exposure capacity is to deploy more commercial tools. Unfortunately commercially available EUV lithography tools (even microfield tools) are prohibitively expensive for resist suppliers and research organizations.

To alleviate exposure capacity shortfall, we propose the development of a low-cost, high-resolution, stand-alone EUV interference lithography (IL) tool. Currently the two operational EUV IL tools in the world are synchrotron based and require coherent illumination making the direct porting of these tools to stand-alone implementations very difficult. Although compact coherent sources [7, 8] seem like the obvious solution for interference lithography, these sources are currently not mature enough to support the near-term needs of EUV resist development. Neither high harmonic nor EUV laser sources have yet to demonstrate the required power and engineering maturity. The best compact-coherent source candidate in terms of engineering maturity, power, and coherence, would be the Colorado State 46-nm laser [8]. Operating this far off from the target wavelength (13.5 nm), however, is clearly not acceptable for the resist-development purposes of this tool. Instead of working with coherent sources, we propose the development of an IL tool capable of utilizing partially coherent illumination.

To the best of our knowledge a total of four different types of IL tools have been implemented at EUV, all of them synchrotron based [5, 9-12]. Presently only one type of system remains in use: the single-grating interference tool [5, 6]. This interferometer type, however, relies on a high degree of spatial coherence making it impossible to port to incoherent sources while maintaining reasonable throughput. Interestingly, two of the previously demonstrated techniques are compatible with incoherent (spatially and temporally) sources. These two techniques are the two-grating interferometer [9] and the re-imaging interferometer [12]. In this paper we present a theoretical study investigating the relative merits of these two approaches.

Emerging Lithographic Technologies XI, edited by Michael J. Lercel,
Proc. of SPIE Vol. 6517, 65172T, (2007) · 0277-786X/07/$18
doi: 10.1117/12.715069

2. HEURISTIC ANALYSIS OF DIFFERENT IL CONFIGURATIONS

As stated above, the single-grating interferometer presently used in the two operational EUV IL tools [5, 6] cannot efficiently be used in non-synchrotron implementations. As with all wavefront division interference systems, this single-grating interferometer requires significant levels of spatial coherence. To avoid the spatial coherence issue, amplitude division systems can be used. The two grating [9] and the re-imaging approaches [12] are examples of amplitude division interference. Moreover, it can be shown that these two systems can also be used with temporally incoherent light. The two incoherent-illumination compatible methods have in common the use of a grating as the beam-splitter. The methods simply differ in the mechanism to recombine the beams. In one case it is a second grating and in the other an imaging optic is used.

We note that not all amplitude division configurations would work with stand-alone incoherent sources. In particular, the Talbot prism type of approach, often used for 193-immersion interference lithography [13], which uses a grating beam-splitter and a prism (or equivalently two flat mirrors) as a beam-combiner, would not work. The reasons for this are discussed below in the analysis of the two-grating configuration.

Next we present more detailed analysis showing that the two-grating and re-imaging methods are indeed viable for use with incoherent light. We begin with the analysis of the re-imaging approach as it is the most intuitive to understand. Figure 1 shows a schematic of such a system depicted, for simplicity, in transmission mode. The imaging optic differs from a conventional optic only in the fact that a central stop is used to block the zero order enabling two-beam interference. Clearly, for an EUV application the lens would be replaced by a reflective optic. The requirement for the central stop makes the use of a Schwarschild type objective the obvious choice. We note that, in principle, a Fresnel Zone Plate could also be used; however, the field of view of such elements would not be sufficient for the application of interest here.

The performance of the re-imaging optic system is intuitive in that it can be viewed simply as a conventional lithography system imaging lines and spaces. Using the central stop to block the zero order from the diffraction grating is basically equivalent to using a chromeless phase-shift mask. In this sense we see that the printed grating will be half the pitch of the beamsplitter grating. Additionally, if the imaging optic has some power, the grating image will be demagnified even further. For example, the Lawrence Berkeley National Laboratory implementation of a coherent version of this interference tool [12] had a total demagnification of 20x. Equating this system to a conventional lithography tool, it is evident that it also works with partially coherent light. The only limitation is that the pupil fill must be smaller than the central obscuration in order to prevent the zero order from propagating through the system. Additionally, the system works with temporally incoherent light since the reflective EUV optic will be achromatic. The drawback of this system is that it requires a relatively high-quality and high-NA EUV optic. To achieve 15-nm lines and spaces, we need an optic with an image-side NA of at least 0.3. Another drawback of this system is that wafer focus control requirements will be just as tight as for a conventional high-NA EUV lithography tool. The primary question for this approach will be the commercial viability related to the cost of the required imaging optic. We note that the optic should have looser specs than, for example, a general lithography optic owing to the fact that the individual diffraction orders will be relatively small in the pupil and that relative phase shifts between the two passed diffraction orders are irrelevant as such errors would simply cause a phase shift of the printed interference pattern.

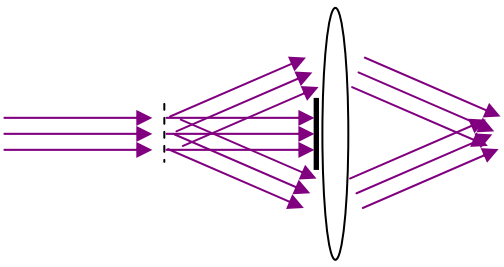

Fig. 1. Schematic of the imaging optic beam-combiner approach. The imaging optic includes a central stop sized large enough to block the entire zero-order pupil fill.

Next we turn to the less intuitive case of the two-grating interferometer. This configuration (Fig. 2) has long been known to support the generation of interference under incoherent (spatially and temporally) illumination [14]. Moreover, these systems have been successfully implemented in a variety of applications [15-18]. Note that we take the term incoherent to be synonymous with partially coherent. Although this is not strictly correct, the physical realization of a fully incoherent illumination (delta-function coherence area) is not possible and all sources we refer to as incoherent

actually generate partially coherent radiation. Spatial coherence is typically viewed as corresponding to the ability of two spatially separated points on a wavefront to interfere. A physical manifestation of this would be a Young's two-pinhole interference test. For spatially coherent light, the pinholes can be arbitrarily far apart and the light will still interfere, whereas with partial coherence there is a limit to the pinhole separation that will allow interference. Keeping one pinhole fixed and mapping out the area that can be covered by the second pinhole while maintaining the ability to interfere gives rise to the concept of coherence area. For isotropic coherence conditions it is fully equivalent to instead consider the lateral coherence length which corresponds simply to the maximum tolerable pinhole separation.

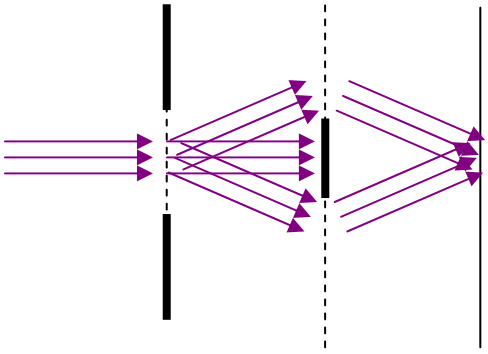

Fig. 2. Schematic of the two-grating interferometer. A second grating is used to recombine the beams separated by amplitude division from the first grating.

It is often more useful to think of spatial coherence as the ability of an optical wavefront to interfere with a laterally shifted or sheared version of itself. This point of view is directly analogous to the concept to temporal coherence which describes the ability of an optical wavefront to interfere with a delayed or longitudinally (temporally) shifted version of itself. Thinking of spatial coherence from this perspective, it is evident that we can indeed interfere spatially incoherent (partially coherent) light provided that it not be sheared by more than the lateral coherence length. Thus when amplitude division is used to split the beam and it is later recombined with little or no shear, interference with incoherent light is possible. Note that the same arguments can be made with broadband light in which case we tend to use common path interferometers to ensure the interfering beams have undergone the same path-length delays thus not incurring any temporal (or longitudinal) shear.

Figure 3 shows how the two-grating interferometer interferes the beam with zero shear. The first grating is used as a beam-splitter. The second grating serves both as a spatial filter and a beam-combiner. The spatial filtering property is used to select only the +/-1 orders from the first grating and +/-1 order diffraction orders from the second grating are used to recombine the beams. Note, thus that the second grating has a frequency of twice that of the first grating. Also, the printed fringe pattern will be of the same frequency as the second grating. This is a drawback compared to the single grating coherent configuration which enables frequency doubling of the beam-combiner grating. This zero shear interference condition occurs only when the interference plane is properly chosen. Figure 4 shows the case where the image plane is defocused. In this case we see that the interfering beams in the image plane come from lateral sheared points in the input plane. Interference can thus only occur if the shear is smaller than the lateral coherence length. This behavior reveals the important property of the limited depth of focus of the two-grating interferometer under partially incoherent illumination.

Although at first blush one might perceive the limited depth of focus as a drawback, it can actually be viewed as a benefit. This property provides a convenient mechanism to emulate defocus in a projection imaging system. Conventional coherent interference lithography tools must use double exposure or branch attenuation methods to achieve contrast reduction emulating defocus. The second benefit of the limited depth of focus of the incoherently illuminated two-grating interferometer is that the image contrast changes throughout the resist stack as it does in conventional lithography systems. Coherent interference systems have an infinite depth of focus, even when the contrast of the fringes is reduced. Finally, noting that the depth of focus is directly proportional to the illumination lateral coherence, one can envision a system where the depth of focus can be adjusted in situ.

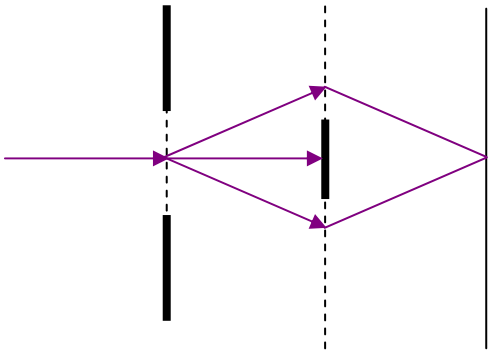

Fig. 3. Assuming the interference plane is properly chosen, the two grating interferometer interferes beam with zero shear.

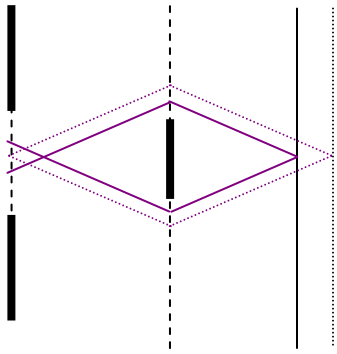

Fig. 4. Defocus in the two-grating interferometer leads to interference of laterally sheared beams. Under incoherent illumination, this leads to a limited depth of focus.

The descriptions above explain how the two-grating interferometer can operate with spatially incoherent light, however, we must also be concerned with temporal incoherence (broadband light). To gain insight into this issue it is instructive to visualize the performance of the system as a function of wavelength. Figure 5 shows the properly focused two-grating interferometer considering two discrete wavelengths. The dashed line represents a longer wavelength. We see that the angular dispersion caused by the first grating is exactly reversed by the second grating. Having the distances properly selected the spatial dispersion thus can be completely eliminated.

Another way to explain the achromatic behavior is to note that 1) the fringe-localization plane (the plane where the spatial shear is nulled and spatially incoherent fringes are possible) is independent of wavelength, 2) the phase of the generated fringe pattern is independent of wavelength (there is no lateral fringe displacement as a function of wavelength), and 3) the increased interference angle as the wavelength is increased exactly cancel each other out such that the frequency of the generated fringe pattern is independent of wavelength.

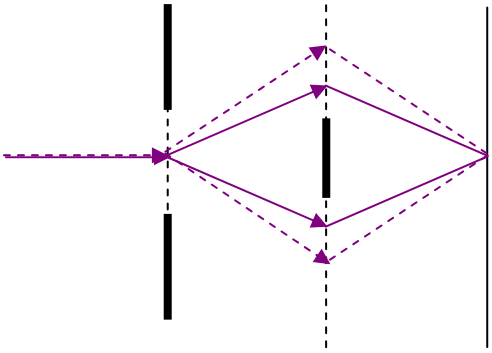

Fig. 5. Achromatic behavior of the two-grating interferometer. Dashed line represents a longer wavelength.

This description leads us naturally to the explanation of why the equivalent of the Talbot prism beam combiner cannot efficiently work with incoherent EUV sources that have relatively broadband illumination. Figure 6 shows such a configuration where the prism is replaced by two flat mirrors for EUV compatibility. Based on the arguments of lateral shear at the interference plane, we see that this configuration remains compatible with spatially incoherent light, however, it is also evident that the configuration is not at all tolerant to broadband light. This is made evident by the strong dependence of the fringe-localization plane on the wavelength. From the same arguments, we also see that the fringe-localization plane is dependent on the frequency of the beam-splitter grating, thus multi-pitch printing in a single exposure is not possible.

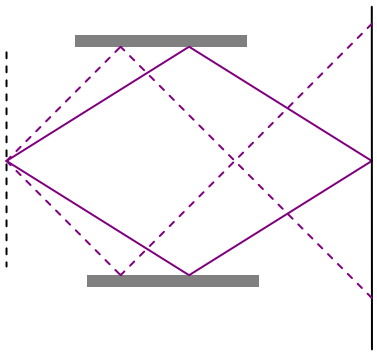

Fig. 6. Schematic of grating beam-splitter and two-mirror combiner configuration. This is equivalent to the Talbot prism combiner configuration. Each color represents a different wavelength. The dashed lines simply represent a different point in the field. Note that the requisite zero-order stop is not shown.

We note that the diagrams above all assume the second grating to have a frequency twice as high as the first. This results in the fringe localization plane distance from the second grating being identical to the distance between the two gratings. This distance-matched condition, however, is not necessary. Choosing the second grating to have some other frequency will simply cause the fringe-localization plane to move. The printed fringe pattern frequency will be equal to 2 times the difference frequency between the two gratings. The factor of two comes from the fact that we are using the +/- 1 orders from the second grating. For the example above where the second grating has a frequency of twice the first (f_2=2f_1), we see that the printed frequency is $2(2f_1-f_1) = 2f_1 = f_2$.

We also note that the grating interferometer need not be limited to two gratings. The system, in principle, works equally well with multiple gratings. A three-grating variant is shown in Fig. 7. The primary benefit of this configuration is that as with the single grating coherent case, the printed fringe pattern frequency is twice that of the gratings. The drawbacks are reduced efficiency and increased complexity. Finally we note that as described by Chang, Alfernez, and Leith [14], a variety of other multigrating configurations are also viable.

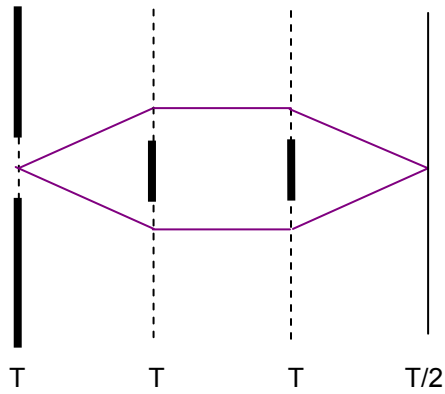

Fig. 7. Schematic of three-grating broad-source achromatic interferometer. The primary benefit here is that the printed fringe pattern frequency is twice that of the gratings.

3. EFFICIENCY AND THROUGHPUT

Finally we turn to the crucial question of efficiency. In the analysis below, we assume the use of a specific commercially available EUV source. Based on cost and performance criteria, the Energetiq EUV source [19] is an excellent candidate for an IL tool. The current standard Energetiq EUV source specification is limited to 10W in 2π steradians and 1% bandwidth. Increasing this specification to 15 W will require a development program primarily devoted to reliability analysis, thermal testing and metrology, and not requiring any extensive redesign in the areas of power delivery or thermal management [20]. Thus we assume the 15 W power level in the efficiency calculations below. We note that the 15W requirement is not primarily based on throughput requirements, but instead is driven by mechanical stability concerns. Various tradeoffs among stability requirements, source power, and overall efficiency are possible.

For obvious reasons, the two-grating design is the case where efficiency is of most concern. The efficiency budget is shown in Fig. 8. We assume a collection angle of +/-10° and a collector comprised of four multilayer reflections with an efficiency of 65% each. Details on the illuminator design are not provided here. We further assume no need for lossy debris mitigation, which we believe to be reasonable based on our experience with the low-debris Energetiq source and our illuminator design. Given the use of gratings, we also suffer a 50% polarization loss. Next we consider the gratings and assume them to be fabricated on approximately 100-nm-thick Nitride membranes. We also assume conventional binary amplitude gratings with 50% duty cycle. Note that the grating efficiency number appears to be high since we use both first orders and are only interested in the effective efficiency in the bright regions of the beam. As stated above, we assume the total source power to be 15 W. Finally, based on our illuminator design, we take the unobstructed beam size at the wafer to be 6-mm in diameter. This all leads to an exposure time of 4.5 seconds for a resist sensitivity of 10 mJ/cm^2.

Considering now the case of the imaging optic beam combiner, we have only one grating but two additional multilayer reflections. Assuming the use of the 5×-reduction optic design, such as the microfield exposure tool (MET) optic [21], we would have the additional significant benefit of demagnification at the image plane. Applying these settings, we find the exposure time to be 0.1 seconds. If we apply the restriction, however, that the field size be 1-mm or larger, we note that fifteen 200x600 μm exposures (the MET optic field size) would have to be stitched together to achieve the desired field size increasing the exposure time to 1.5 seconds, ignoring stage motion requirements. We see that the benefit of the imaging-optic design lies in its demagnification and can only be realized if smaller field sizes are acceptable. Noting that the field size would simply be that of existing microfield EUV exposure tools, this does not appear to pose a significant problem.

collection efficiency	0.015192247		collection angle= 10 degrees
M1 (illuminator)	0.65		
M2 (illuminator)	0.65		
M3 (illuminator)	0.65		
M4 (illuminator)	0.65		
Polarization loss	0.5		
grating 1 membrane	0.5		100-nm Nitride membrane
grating 1 diffraction	0.405284735		binary amplitude (consider efficiency of bright areas only)
grating 2 membrane	0.5		100-nm Nitride membrane
grating 2 diffraction	0.405284735		
TOTAL	**5.57E-05**		
input power	15000	mW	
power at wafer	8.35E-01	mW	
area at wafer	0.36	cm^2	
wafer power density	2.320	mW/cm^2	
exposure time	4.3	seconds	resist sensitivity= 10 mJ/cm^2

Fig. 8. Efficiency determination for dual grating IL system.

4. DEPTH OF FOCUS

Next we explicitly consider depth of focus. As stated above, fringes are only obtained when the image plane is properly positioned to meet the zero-shear condition. By similar arguments, the depth of focus can be predicted by determining the longitudinal position range of the image plane over which the beam shear is smaller than the coherence width. It is evident that the shear angle is directly proportional to the grating pitch, thus as one should expect the depth of focus will vary as a function of pitch and coherence area. The coherence width is determined by the source size and the numerical aperture of the illuminator. Although not presented here, the illuminator introduced in the previous section provides a coherence width (W_c) of 275 nm. This width could readily be increased, however, this would come at the cost of efficiency. Conversely, we could improve the throughput of the system by accepting a smaller coherence width, however, this would come at the cost of complexity for the illuminator. We believe the value we have chosen to

represent a reasonable tradeoff. Assuming target fringes of 15-nm half-pitch, the relative shear angle between the two interfering beams can be shown to be 26°. Using these values, we find the depth of focus to be

$$DOF = W_c/\tan(26°) = 564 \text{ nm}. \quad (1)$$

We note that this value has been verified both through rigorous physical optics analysis as well as computer modeling.

For comparison purposes, we also determine the depth of focus for the re-imaging case. Although in one sense this system is just conventional lithography, it is being used with rather unconventional settings (partial coherence of 0.11 with the zero order being fully blocked by the central obscuration). For this reason we use lithographic modeling software to determine the depth of focus rather than relying on the conventional equation of $0.5\lambda/NA^2$. Using this software and assuming the printing of 15-nm half pitch fringes, we find a depth of focus of 570 nm, essentially identical to the value for the two-grating interferometer.

5. SUMMARY

We have presented two possible configurations for a stand-alone EUV IL tool based on the use of a conventional incoherent source. The two methods share in common the fact that a grating is used as the primary beam-splitter and that an on-axis low-image-side-NA illuminator is used. Both systems provide a large, but not infinite, DOF. Although not discussed here, the two-grating approach has the benefit of the largest flexibility in terms of simultaneous pitch printing. The major drawbacks of the method are tight alignment tolerances and strict quality requirements on the gratings. We are currently performing a detailed analysis of both these areas.

The imaging-optic approach has the benefit of being essentially a proven technology since it can be viewed simply as a conventional projection lithography system. The method suffers, however, from cost concerns related to the price of the high-NA high-quality EUV optic required as the beam-combiner. Also, if large field sizes are required, this method would suffer from throughput concerns.

REFERENCES

1. R. Stulen and D. Sweeney, "Extreme ultraviolet lithography," IEEE J. Quantum Electron. **35**, 694-699 (1999).
2. P. Naulleau, K. Goldberg, E. Anderson, K. Bradley, R. Delano, P. Denham, B. Gunion, B. Harteneck, B. Hoef, H. Huang, K. Jackson, G. Jones, D. Kemp, A. Liddle, R. Oort, A. Rawlins, S. Rekawa, F. Salmassi, R. Tackaberry, C. Chung, L. Hale, D. Phillion, G. Sommargren, J. Taylor, "Status of EUV microexposure capabilities at the ALS using the 0.3-NA MET optic," Proc. SPIE **5374**, 881-891 (2004).
3. A. Brunton, J. Cashmore, P. Elbourn, G. Elliner, M. Gower, P. Grunewald, M. Harman, S. Hough, N. McEntee, S. Mundair, D. Rees, P. Richards, V. Truffert, I. Wallhead, M. Whitfield, "High-resolution EUV microstepper tool for resist testing and technology evaluation," Proc. SPIE **5448**, 681-692 (2004).
4. H. Oizumi, Y. Tanaka, I. Nishiyama, H. Kondo, K. Murakami, "Lithographic performance of high-numerical-aperture (NA=0.3) EUV small-field exposure tool (HINA)," Proc. SPIE **5751**, 102-109 (2005).
5. H. H. Solak, C. David, J. Gobrecht, V. Golovkina, F. Cerrina, S. O. Kim, P. F. Nealey, "Sub-50 nm period patterns with EUV interference lithography," Microelectronic Engineering, **67**, 56 (2003).
6. H. H. Solak, "Nanolithography with coherent extreme ultraviolet light," J. Phys. D: Appl. Phys. **39,** 171 (2006).
7. X. Zhang, A.R. Libertun, A. Paul, E. Gagnon, S. Backus, I.P. Christov, M.M. Murnane, H.C. Kapteyn, R.A. Bartels, Y. Liu, D.T. Attwood, "Highly Coherent Light At 13 Nm Generated By Use Of Quasi-Phase-Matched High-Harmonic Generation", Optics Letters **29,** 1357, (2004).
8. S. Heinbuch, M. Grisham, D. Martz, and J.J. Rocca, "Demonstration of a desk-top size high repetition rate soft x-ray laser", Optics Express, **13**, 4050, (2005).
9. M. Wei, E. Gullikson, J.H. Underwood, T.K. Gustafson, and D.T. Attwood, "White-Light Spatial Frequency Multiplication Using Soft X-Rays" SPIE **2516**, 233 (1995).
10. H. H. Solak, D. He, W. Li, S. Singh-Gasson, F. Cerrina, B. H. Sohn, X. M. Yang, P. F. Nealey, "Exposure of 38 nm period grating patterns with extreme ultraviolet interferometric lithography," Appl. Phys. Lett., **75**, 2328 (1999).
11. H. H. Solak, C. David, J. Gobrecht, V. Golovkina, F. Cerrina, S. O. Kim, P. F. Nealey, "Sub-50 nm period patterns with EUV interference lithography," Microelectronic Engineering, **67**, 56 (2003).
12. M. Shumway, S. Lee, C. Cho, P. Naulleau, K. Goldberg, and J. Bokor, "Extremely fine-pitch printing with a 10× Schwarzschild optic at extreme ultraviolet wavelengths," Proc. SPIE **4343,** 357-362 (2001).

13. Anatoly Bourov, Yongfa Fan, Frank C. Cropanese, Neal V. Lafferty, Lena Zavyalova, Hoyoung Kang, Bruce W. Smith, "Immersion microlithography at 193 nm with a Talbot prism interferometer," Proc. SPIE **5377,** 1573-1578 (2004).
14. B. J. Chang, R. Alfernez, and E. N. Leith, "Space-invariant achromatic grating interferometers: theory," Appl. Opt. **14**, 1592 (1975)
15. D. Angell, "Incoherent spatial filtering with grating interferometers," Appl. Opt. **24**, 2903 (1986).
16. E. N. Leith, D. Angell, and C. P. Kuei, "Super-resolution by coherent-to-incoherent conversion," J. Opt. Soc. Am. A **4**, 1050 (1987).
17. P. C. Sun and E. N Leith, "Broad-source image plane holography as a confocal imaging process," Appl. Opt. **33**, 597-602 (1994).
18. P. Naulleau, C. Chen, and E. Leith, "Analysis of direct 3-D image transmission through optical fibers by use of coherence methods," Appl. Opt. **35**, 3953-3962 (1996).
19. Stephen F. Horne, Matthew M. Besen, Donald K. Smith, Paul A. Blackborow, Robert D'Agostino, "Application of a high-brightness electrodeless Z-pinch EUV source for metrology, inspection, and resist development," Proc. SPIE **6151**, 201-210 (2006).
20. P. Blackborow, D. Gustafson, D. Smith[1], M. Besen, S.Horne, R. D'Agostino, Y. Minami, G. Denbeaux, "Application of the Energetiq EQ-10 Electrodeless Z-PinchTM EUV Light Source in Outgassing and Exposure of EUV Photoresist," *these proceedings*.
21. J. Taylor, D. Sweeney, R. Hudyma, L. Hale, T. Decker, G. Kubiak, W. Sweatt, N. Wester, "EUV Microexposure Tool (MET) for near-term development using a high NA projection system," 2nd International EUVL Workshop October 19-20, 2000, proceedings available from SEMATECH, Austin, TX.